Original Article

MOLECULAR METABOLISM

Permanent neonatal diabetes-causing insulin mutations have dominant negative effects on beta cell identity

Yuwei Zhang [1,5], Lina Sui [1,5], Qian Du [1], Leena Haataja [2], Yishu Yin [1], Ryan Viola [1], Shuangyi Xu [1], Christian Ulrik Nielsson [1], Rudolph L. Leibel [1], Fabrizio Barbetti [3,4], Peter Arvan [2], Dieter Egli [1,*,6]

ABSTRACT

Objective: Heterozygous coding sequence mutations of the *INS* gene are a cause of permanent neonatal diabetes (PNDM), requiring insulin therapy similar to T1D. While the negative effects on insulin processing and secretion are known, how dominant insulin mutations result in a continued decline of beta cell function after birth is not well understood.

Methods: We explored the causes of beta cell failure in two PNDM patients with two distinct *INS* mutations using patient-derived iPSCs and mutated hESCs.

Results: we detected accumulation of misfolded proinsulin and impaired proinsulin processing *in vitro*, and a dominant-negative effect of these mutations on beta-cell mass and function after transplantation into mice. In addition to anticipated ER stress, we found evidence of beta-cell dedifferentiation, characterized by an increase of cells expressing both Nkx6.1 and ALDH1A3, but negative for insulin and glucagon.

Conclusions: These results highlight a novel mechanism, the loss of beta cell identity, contributing to the loss and functional failure of human beta cells with specific insulin gene mutations.

Keywords Insulin; ER stress; iPS cells; Gene correction; Cell therapy; Beta cell de-differentiation; Permanent neonatal diabetes

1. INTRODUCTION

Neonatal Diabetes Mellitus (NDM) is a rare disorder with an incidence of about 1/100,000 live births; approximately 50% of cases are permanent (PNDM) [28]. Heterozygous coding sequence mutations of the insulin (*INS*) gene are among the leading causes of PNDM [13,15,17,62]. In Western Europe and the U.S., mutations in *KCNJ11*, *INS* and *ABCC8* account for about 65–70% of PNDM cases [22]. Other causes are structural abnormalities on chromosome 6q24, as well as biallelic *GCK* and *PDX1* mutations, but the latter are exceedingly rare [15]. In the Middle East, the leading gene is *EIF2AK3* causing Wolcott–Rallison syndrome, followed by mutations in other recessive genes, including *PTF1A* and biallelic recessive *INS* mutations [25]. PNDM is usually diagnosed within 6 months of birth, presenting variously as mild hyperglycemia with failure to thrive or fatal diabetic ketoacidosis (DKA) [13,14,16,30,52].

Diabetic mouse models segregating for dominant *INS* gene mutations, such as the Akita ($INS2^{+/C96Y}$) and Munich ($INS2^{+/C95S}$) mice have been studied to elucidate the molecular pathogenesis of the resulting diabetes, as their early-onset diabetic phenotypes resemble human PNDM [26,32,48,70,76]. Disrupted proinsulin folding and activated endoplasmic reticulum (ER) stress have been implicated in these heterozygous mutant mice. Transfection of mutated insulin transcripts nominally affecting protein folding in beta cell lines causes cell death [13]. In all of these models, the presence of a non-mutant *INS* allele does not rescue the beta cell failure phenotype [72].

Proinsulin folding occurs primarily within the ER. Native proinsulin folding is associated with the formation of three specific disulfide bonds pairing 6 cysteines (A6–A11, A7–B7, and A20–B19; A: A chain, B: B-chain) [71]. Conserved among most members of the insulin superfamily, these disulfide bridges are critical to the 3-dimensional structure of proinsulin and the bioactivity of insulin [41]. *INS* mutations affecting cysteine residues can directly interfere with proper proinsulin disulfide bond formation [13,31,75]; and various non-cysteine mutations can also impair cysteine alignment leading to defective disulfide bond formation [13,23,26]. Increased accumulation of misfolded proinsulin invokes ER chaperone proteins such as BIP/GRP78 and GRP94 [41,48]. Pancreatic beta-cells are susceptible to perturbations of ER homeostasis which can cause cell death in mice with insulin mutations [48], T2D and possibly T1D [8]. However, direct

[1]Naomi Berrie Diabetes Center & Department of Pediatrics, College of Physicians and Surgeons, Columbia Stem Cell Initiative, Columbia University, New York, NY, 10032, United States [2]Metabolism Endocrinology & Diabetes, University of Michigan, Ann Arbor, MI 48105, United States [3]Department of Experimental Medicine, University of Rome Tor Vergata, Rome 00133, Italy [4]Monogenic Diabetes Clinic, Endocrinology and Diabetes Unit, Bambino Gesù Children's Hospital, Rome 00164, Italy

[5] These authors contributed equally.
[6] Lead contact.

*Corresponding author. E-mail: de2220@cumc.columbia.edu (D. Egli).

Received October 6, 2023 • Revision received January 8, 2024 • Accepted January 9, 2024 • Available online 16 January 2024

https://doi.org/10.1016/j.molmet.2024.101879

proof that ER stress triggers programmed beta-cell death in diabetic patients (or in PNDM infants) is lacking [55,74].

Patient-derived human induced pluripotent stem cells (hiPSCs) can be differentiated to pancreatic beta-cells (SC beta-cells), offering the prospect of replacement cell therapy for both T1D as well as for monogenic forms of diabetes [9,33]. Many studies have shown the value of stem cell models of monogenic forms of diabetes for gaining understanding of the pathophysiology of more prevalent types of diabetes mellitus [1].

Endoplasmic reticulum (ER) stress affects insulin biosynthesis and secretion in stem cell derived beta cells [5,44,56]. In the present study, we sought to understand mechanisms driving beta cell failure associated with two distinct pathologic *INS* mutations: $L^{B15}Y^{B16}$delinsH and $Y^{B26}C$ (current nomenclature according to Human Genome Variation Society: p.Leu39_Tyr40delinsHis and p.Tyr50Cys), using differentiation of human iPSCs and embryonic stem cells (hESCs). We corrected patient-derived iPSCs using CRISPR/Cas9 to create isogenic controls, along with WT iPSCs and hESCs as additional controls. Differentiation efficiency, and short-term proinsulin/insulin synthesis and proinsulin foldability were examined *in vitro*. Development and maintenance of beta-cell identity, as well as ER stress, were assessed *in vivo* upon transplantation of stem cell-derived beta cells into immunodeficient mice. Collectively, our findings indicate that specific heterozygous *INS* mutations in human beta cells cause diabetes by dominant-negative effects on insulin biosynthesis and secretion, as well as through a newly identified mechanism: de-differentiation and loss of beta-cell identity.

2. RESULTS

2.1. Two patients segregating for *INS* mutations with distinct neonatal diabetes syndrome

A female neonate (Policlinico Tor Vergata **PTV1**) born at term (birth weight: 3350 g) after an uneventful pregnancy was diagnosed with diabetic ketoacidosis (DKA) at 37 days of age; plasma glucose 613 mg/dL and arterial blood pH 7.22 [13]; (kindred D), (Figure 1A). T1DM-related autoantibody status is unknown. Plasma C-peptide was low but measurable up to one year of age and subsequently became undetectable. Insulin administration was initiated at the time of diagnosis (d37) with a full dose at 1 UI/kg/d with good metabolic control (mean HbA1c 7.3% from 1994 to 2013). Currently at age 24, she remains free of diabetic complications (Figure 1A) [29]; case #2). A second patient (**PTV2**; a female with a birth weight of 2500 g) was diagnosed with diabetes (plasma glucose 509 mg/dL) at one month of age, without accompanying ketoacidosis or other complications [47]; plasma C-peptide (0.47 ng/l). The patient was treated with continuous subcutaneous insulin infusion (0.7 UI/kg/d) and discharged uneventfully. Good metabolic control without complications (mean HbA1c 6.4%) has been maintained up to the present age of 8 years (Figure 1A

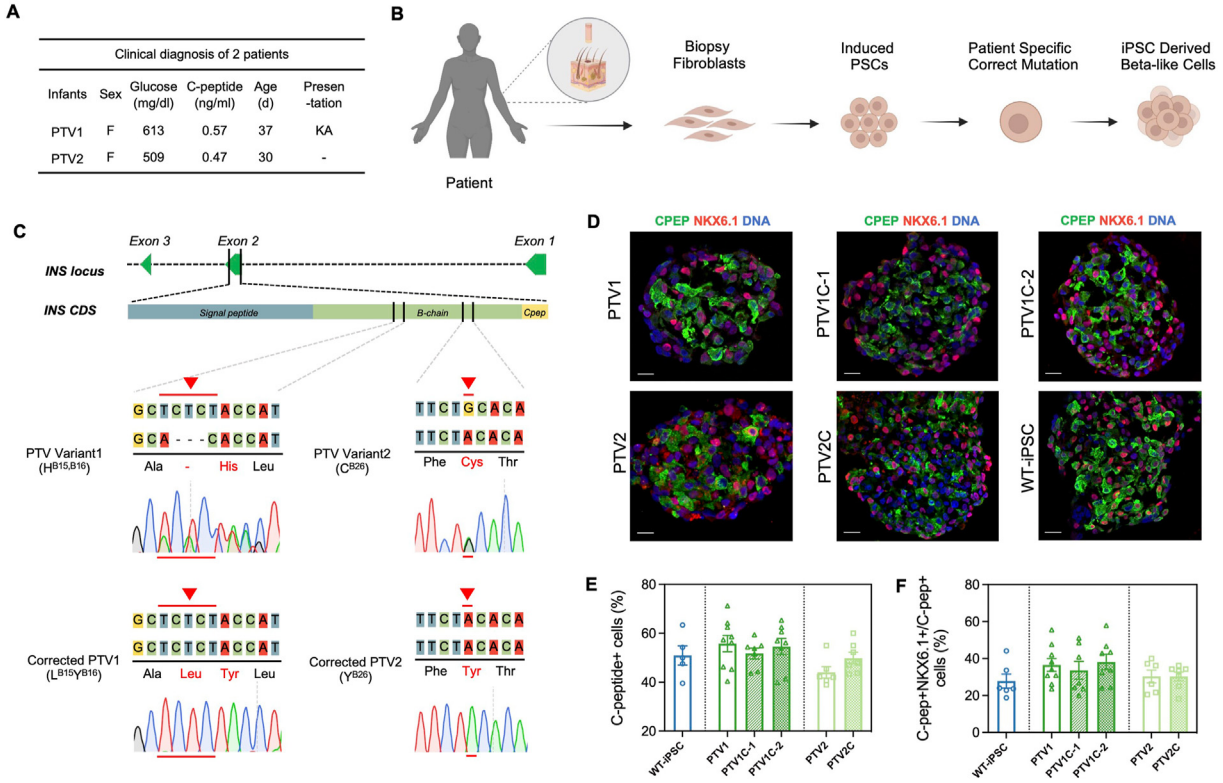

Figure 1: Generation of neonatal diabetes disease models with insulin mutations and their isogenic controls. (A). Diagnosis of two permanent neonatal diabetes (PNDM) patients segregating formutations in the insulin gene (*INS*). Age at diagnosis is shown, with corresponding glucose levels, and symptoms. C-peptide concentrations were measured at day 40 for PTV1 and day 37 for PTV2. PTV: Policlinico Tor Vergata patient variant; F: female; KA: Ketoacidosis. **(B)**. A schematic of the PNDM model. Patient fibroblasts are reprogrammed to iPS cells, isogenic controls were made by gene correction, and both mutant and corrected cells were differentiated to beta-like cells. **(C)**. Molecular identity of patient variants PTV1 and PTV2 and CRSPR/Cas9-corrected isogenic controls were examined by DNA sequencing. **(D)**. Immunostaining of frozen sections of PTV1 and corrected PTV1C, PTV2 and PTV2C, and WT iPSC-derived beta cell clusters at d27 for C-peptide (the antibody detects both C-peptide and aa 33–63 of proinsulin), NKX6.1. Scale bar: 20 μm. **(E)**. Quantitation of beta cell differentiation efficiency indicated by C-peptide+ population (%) and **(F)** C-peptide+ cells co-expressing NKX6.1 population (%). n = 5–9 independent differentiation experiments per genotype. Respective cell numbers quantified in cell blocks with a mean of ~130 cells per block and presented as mean ± SEM. One-way ANOVA with *: $P < 0.05$.

and Table S1). However, C-peptide levels were halved within six months of diagnosis, and were barely detectable by age 6 years. The phenotype of both patients is consistent with declining function of beta cells over time.

2.2. *INS* mutant iPSC lines efficiently generate insulin-producing cells

We generated patient-specific iPSC cell lines by reprogramming skin fibroblasts of the two patients (designated PTV1 and PTV2; Figure 1B). The patients carried distinct heterozygous mutations: an in-frame substitution in which B-chain Leu15 and Tyr16 are replaced by a single His residue ($L^{B15}Y^{B16}$delinsH; **PTV1**); a point mutation in which B-chain Tyr26 is replaced by Cys ($Y^{B26}C$, adding an additional cysteine to the B chain **PTV2**). We established 3 isogenic control cell lines by correcting the mutation of patient-derived iPSCs with CRISPR/Cas9: 2 corrected cell lines edited from **PTV1** (denominated **PTV1C-1** and **PTV1C-2**), and 1 corrected cell line from PTV2 (denominated **PTV2C**) (Figure 1C).

We differentiated 6 iPSC lines: 2 patient-derived iPSCs, 1 non-isogenic healthy control WT-iPSCs (line # 1159, from donors without diabetes) and 3 isogenic control iPSC lines into SC-derived beta cells using a previously published protocol [64]. The differentiation protocol is outlined in Figure S1A. All cell lines were differentiated into islet-like clusters containing insulin-expressing cells and were karyotypically normal (Figure S1B, C).

We characterized the islet-like clusters by immunochemistry and flow cytometry for beta cell markers: C-peptide and NKX6.1. Equivalent percentages (~50%) of C-peptide-positive cells were detected among all the cell lines (Figures 1D, E and S1B). For **PTV1**, 36% of cells co-expressed both C-peptide+ and NKX6.1, similar to isogenic controls including **PTV1C-1** (34%) and **PTV1C-2** (38%). The percentage of NKX6.1+/C-peptide+ double-positive cells in **PTV2** patient cell lines with (**PTV2C**) or without correction was 30% and not significantly different from other lines (Figures 1D, F and S1B). These data suggest that PTV1 and PTV2 mutations do not affect cellular developmental ability to generate pancreatic beta-like cells.

2.3. Defective proinsulin processing, insulin formation, and secretion in patient-derived beta cells

To determine if these *INS* mutations affect insulin production in differentiated stem cell derived beta cell clusters on d27, we examined proinsulin and insulin levels by immunoassay in PTV1 and PTV2 cells, their isogenic controls (PTV1C-1, PTV1C-2, and PTV2C) and WT iPSCs. Our prior findings indicated a lower insulin content and comparable proinsulin levels between SC-derived islets and primary islets. Furthermore, the ratio of proinsulin/insulin content is lower in primary human beta cells, though the difference was not significant [63]. Though the experimental system used here is not identical to mature primary pancreatic beta cells, we are comparing within a consistent experimental system. Using this system, we observed that PTV1C-1, PTV1C-2 cells produced more proinsulin and insulin compared to PTV1 and PTV2 cells (Figure 2A, B). We also evaluated expression of proinsulin and insulin in SC-clusters by immunostaining (Figure S2A). A similar percentage of proinsulin positive cells was detected in each genotype (Figure S2B). However, the insulin producing cell number was reduced in SC-clusters with PTV1 mutation ($H^{B15, B16}$) compared to isogenic controls, and a similar trend was observed in clusters with the PTV2 mutation (C^{B26}) (Figure S2C). The ratio of proinsulin to insulin immunopositive cells was significantly higher in both patient-derived sc-clusters, suggesting that these mutations may be associated with deficient insulin formation from proinsulin (Figure S2D).

We introduced the PTV1 mutation ($H^{B15, B16}$) into the Mel1 human embryonic stem cell line (**Mel1-WT**) and generated two hemizygous cell lines (**Mel1-PTV1-1** and **Mel1-PTV1-2**) and one insulin knock out cell line as a negative control (**Mel1-INS KO**). Several attempts to introduce the PTV2 mutation into the Mel1 ESC line were unsuccessful. Genotypes of the 4 cell lines used are illustrated in Figure 2C, and Figure S3A. Because Mel1 cells carry an inactivating GFP knock-in on one of the insulin alleles [45], Mel1-derived cell lines express only a mutant protein, while patient cells express both a wild type and a mutant protein (Figures 2C, S3A–E). These mutant Mel1 cell lines differentiated to beta-like cells with efficiency comparable to that of unmanipulated Mel1 cells, as quantified by flow cytometry using an antibody recognizing C-peptide (including cleaved C-peptide and aa 33–63 of proinsulin) and Nkx6.1, and GFP fluorescence (Figure S3F and G). Insulin knockout cell lines expressed GFP, but no insulin (Figure S3H). All cell lines had normal karyotypes (Figure S3I). Similar to patient iPSCs, Mel1 cells carrying a PTV1 mutation were immunopositive for proinsulin, and only weakly insulin immunopositive (Figure S3J and K).

To assess proinsulin processing in the mutant cells we performed Western blotting for processing intermediates. Normally, upon excision of the preproinsulin signal peptide in the endoplasmic reticulum, proinsulin disulfide bridges form between specific cysteine residues, followed by intracellular transport of proinsulin to secretory granules in which proinsulin is cleaved by PCSKs to generate mature insulin [42] (Figure 2D).

We quantified synthesis of proinsulin, its processing to insulin and the secretion of insulin. Stem cell derived beta cells (sc-beta) PTV1 cells were pulse-labeled using ^{35}S-amino acids, and chased for either 5 min or 90 min. At 5 and 90 min, proinsulin and insulin were immunoprecipitated with anti-insulin and analyzed by nonreducing SDS-PAGE. Whereas gene-corrected PTV1C cells formed native proinsulin, the uncorrected patient cells exhibited a proinsulin band of abnormal mobility (i.e., non-native), detected after both 5 min and 90 min of chase (Figure 2E). Additionally, whereas the gene-corrected cells synthesized and secreted insulin, in the PTV1 patient cells, formation and secretion of labeled insulin was markedly impaired (Figure 2E). These data are consistent with defects in proinsulin folding and insulin formation in PTV1 sc-derived beta cells.

Misfolding of proinsulin monomers can promote the formation of aberrant intermolecular proinsulin disulfide bonds [3,4,23,66]. We examined this possibility using anti-proinsulin immunoblotting of protein extracts from stem cell derived beta cell clusters, and resolved by nonreducing SDS-PAGE. All genotypes were examined, including normal controls, heterozygous mutant, and corrected patient cells for both variants, as well as PTV1 hemizygous mutant ESCs and controls. In cells carrying at least one copy of WT *INS* (WT iPSC, PTV1, PTV1C, PTV2, PTV2C and Mel1-WT), proinsulin was detected in two bands near the 6 kD molecular mass marker, representing intact proinsulin (lower band) and a proinsulin conversion intermediate (upper band), a pattern consistent with proinsulin folding, trafficking, and ongoing maturation in the secretory pathway (Figure 2F). In contrast, no normal proinsulin (or intermediate) bands were found in samples carrying only the mutant *INS* copy (Mel1-PTV1-1 and Mel1-PTV1-2). These two cell lines had only a proinsulin band of abnormal mobility, consistent with defective proinsulin monomer folding and an inability of that proinsulin to undergo normal trafficking and maturation in the secretory pathway (Figure 2F). Consistent with these findings, by reducing SDS-PAGE, cells containing a wild type copy showed the presence of a processed insulin B-chain, confirming the ability of proinsulin to undergo trafficking and maturation in the secretory pathway. Whereas in cells bearing only a mutant PTV1 allele, this pattern was not observed

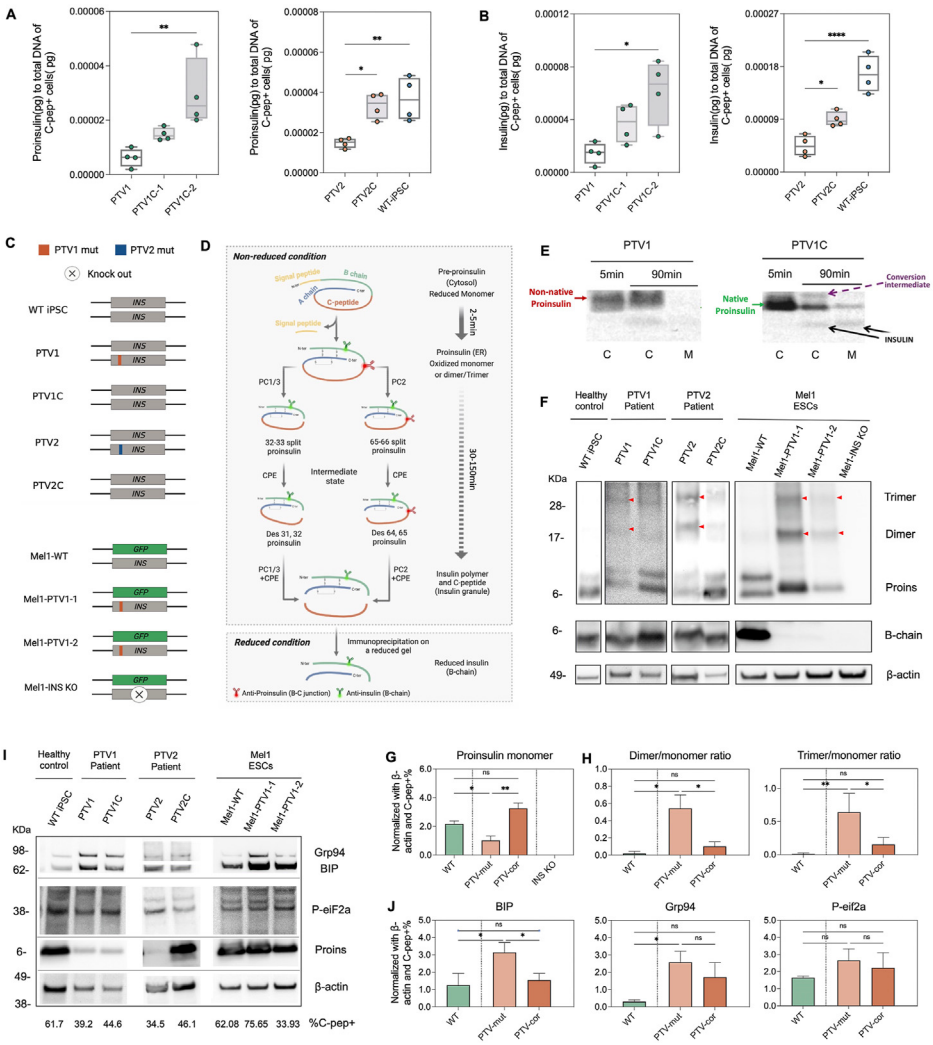

Figure 2: Reduced Proinsulin and insulin production in *INS* mutants accompanied by elevated ER stress and UPR. (A) Human proinsulin content and **(B)** insulin content in sorted SC-beta cells clusters derived from WT iPSC, PTV mutants (PTV1 and PTV2) and their isogenic controls (PTV1C-1, PTV1C-2 and PTV2C). Content was normalized to the percentage of insulin-positive cells determined by flow cytometry. n = 4 per genotype. Data plots are presented as mean ± SEM. One-way ANOVA test with $^{*}P < 0.05$, $^{**}P < 0.01$, $^{***}P < 0.001$, $^{****}P < 0.0001$. **(C)** Genotypes of iPSC lines and Mel1-hESC lines. Insulin-expressing allele is shown in gray; GFP allele is shown in green. PTV1 and PTV2 mutations are indicated respectively by orange and blue bars. **(D)** Schematic of insulin processing. Uncleaved pre-proinsulin in a reduced monomer form is processed to proinsulin, which is then cleaved to intermediates in the ER visible as double proinsulin bands on a non-reducing gel in the process of cleavage of proinsulin to insulin. Intermediate state: The junctions of the B and A chains, between residues 32 and 33 (R↓E) and residues 65 and 66 (R↓G) are recognized by the neuroendocrine convertases PC1/3 and PC2, respectively, during initial processing cleavages to form split-proinsulin. The resulting cleavage products extend insulin at the B chain C terminus through R31-R32 and extend C-peptide C-terminally through K64-R65. Subsequently, carboxypeptidase E (CPE) trims these products by removing the basic residues to form des-proinsulin (Top). A reducing gel shows only the processed B chain with the antibody used (Bottom). Illustrated using Biorender. **(E)** Pulse-chase experiment using non-reducing gel. Western blot for insulin using an antibody specific to B-chain for cellular content and secretion. Misfolded non-native proinsulin with abnormal disulfide linkages (red arrow), normally folded proinsulin (green arrow, below), conversion intermediate of proinsulin to insulin (purple arrow) and insulin (black arrow). C: samples collected from cells; M: samples collected from media to detect secreted insulin. Note that only gene-corrected cells process and secrete insulin efficiently. **(F)** Western blots showing the processing of non-reduced proinsulin monomer (Proins) and distinct higher molecular weight bands corresponding to dimeric and trimeric proinsulin (dimer and trimer) indicating intermolecular disulfide bond formation in mutants (Top area). Anti-proinsulin antibody specifically detecting B—C junction sequence KTRREAEDLQ was used to detect non-reduced proinsulin, hence the "Proins" bands denote the normally processed monomers. This antibody detects a mutant protein in MEL-1cells.The expression of processed B-chain recognized by an anti-Insulin antibody binding on B-chain is shown using a reducing gel below. **(G—H)** Quantitation of Western blot for proinsulin processing products. For quantification purpose, the WT iPSC and Mel1-WT groups were consolidated into the WT group; four cell lines displaying PTV mutation (PTV1, PTV2, Mel1-PTV1-1, Mel1-PTV1-2) were merged into the PTV-mut group; two isogenic (corrected) controls (PTV1C and PTV2C) were combined as the PTV-cor group. **(G)** Proinsulin monomer is normalized with β-actin and differentiation efficiency quantified by flow cytometry for the percentage of C-peptide positive cells (%C-pep+). **(H)** Trimer/monomer and dimer/monomer ratio as an indication of proinsulin to insulin processing failure in PTV mutant cells. **(I)** Representative Western blots showing ER stress markers including Grp94, BIP, P-eiF2a and proinsulin expression in all lines. Normalized with β-actin. Additionally, quantification is normalized to differentiation efficiency (C-pep+), which was above 40% for all samples. Lanes are denominated by their origins (WT iPSCs from a healthy control. PTV1 and its isogenic control PTV1C from patient carrying PTV1 mutation, PTV2 and PTV2C from another patient with PTV2 mutation. WT-MEL1, Mel1-PTV1-1 and Mel1-PTV1-2 from Mel1-hESC). All lanes stained for different proteins are from the same membrane. **(J)** Quantitation of Western blot for ER stress proteins. WT includes WT iPSC and Mel1-WT; PTV-mut comprises PTV1, PTV2, Mel1-PTV1-1, Mel1-PTV1-2; PTV-cor includes PTV1C and PTV2C.

(Figure 2F). Thus, the variant PTV1 mutation ($H^{B15, B16}$) is incompatible with the formation of mature insulin.

We also detected aberrant disulfide-linked proinsulin dimers and trimers within patient-derived and Mel1-derived beta-like cells bearing the PTV1 *INS* mutation (Figure 2F). Though these complexes were also seen in wild type cells, PTV1 mutant cells showed decreased proinsulin monomer per insulin-positive cell (Figure 2G, Table S2), and an increased ratio of proinsulin trimer and dimer to monomer, especially in the sc-derived beta-like cells expressing the proinsulin mutant (PTV2) bearing the extra cysteine residue (Figure 2H, Table S2). These aberrant signals are allele-specific, as insulin knockout cells do not show either monomeric or oligomeric proinsulin signals despite their ability to differentiate (Figure 2F).

These data demonstrate that the PTV mutations interfere with proper formation of disulfide bonds and increase aberrant disulifide-linked proinsulin dimers and trimers, resulting in diminished proinsulin endoproteolytic processing due to defective anterograde proinsulin trafficking in the secretory pathway. These derangements contribute to reduced insulin production in *INS* mutant cells.

2.4. Increased ER stress in insulin mutant sc-beta cells

Retention of proinsulin in the ER has previously been reported in Akita mice segregating for a tertiary structure-altering missense mutation (Cys96Tyr) of *INS2* [13,48]. We assessed ER stress in sc-derived beta cell clusters (at 27d of *in vitro* differentiation) by assaying protein levels of BIP, GRP94 and phospho-eiF2α. By Western blotting, we found only a modest activation of ER stress pathways: BIP and GRP94 exhibited an increase in mutant PTV cell lines (Figure 2I), and a decrease upon correction, though the effect was small, but significant when considering all genotypes (Figure 2J, Table S2). In contrast, the normally folded proinsulin is increased after gene correction as the dimerization and trimerization of proinsulin effectively reversed in PTV corrected cells (Figure 2F, I and J). Specifically, in patient iPSC-derived beta cell clusters carrying PTV1 and PTV2 mutations, immunofluorescence of BIP was increased in insulin-positive cells (Figure S4A and C). Likewise, Mel1 cells carrying a PTV1 mutation also showed an increased number of BIP/insulin double-positive cells (Figure S4B and D). These data suggest that - as in Akita mouse beta cells - impaired folding of proinsulin results in increased ER stress which decreases insulin production [38].

2.5. Reduced C-peptide secretion in patient-derived beta cell grafts transplanted in NSG mice

We tested the function of patient-derived SC-beta cells *in vivo*, by grafting these cells into immunodeficient NSG mice. We transplanted $1\sim2\times10^6$ beta cells from mutant, isogenic gene-corrected controls, and WT controls, into the gastrocnemius muscle of NSG mice. Beta cells grafted into mice display physiologic glucose-stimulated insulin secretion, allowing detailed functional interrogation of specific beta cell genes [65]. Here, we monitored human C-peptide secretion in the fed state and after intraperitoneal glucose challenge.

In mice engrafted with WT iPSC (1159)-derived or ESC (Mel1)-derived cells, interim serum concentrations of human C-peptide in the random (fed) state rose gradually to 1248 pM in Mel1-WT engrafted mice or 1210 pM in WT-iPSC (Figure 3A). This time course suggests that the SC-derived beta cells integrated with the mouse vascular system and were maturing *in vivo*. In contrast, NGS mice transplanted with PTV1 or PTV2 grafts showed detectable but extremely low random C-peptide concentrations post-transplantation (Figure 3A). We also examined random mouse C-peptide concentrations at 7 months after grafting. As expected, secretion of mouse C-peptide in WT SC-islets engrafted mice was suppressed due to insulin secretion from the human beta cell grafts. In PTV SC-islets engrafted mice, high levels of mouse C-peptide persisted, consistent with a failure of human insulin secretion in these animals (Figure 3B, C). Thus, whereas a single wild type insulin gene is sufficient in MEL-1 cells to regulate mouse blood glucose levels, cells with a single wild type insulin allele in combination with a mutant insulin allele fail to secrete physiologically sufficient amounts of insulin. These data are consistent with a dominant-negative impact of structural mutations of proinsulin molecules on the function of patient-derived SC-beta cells *in vivo*.

To further assess the metabolic physiology of mice transplanted with beta cells expressing mutant or corrected *INS*, mice were fasted overnight and then challenged with intraperitoneal glucose (2 g/kg body mass). Mice engrafted with PTV1 or PTV2 cells displayed impaired human C-peptide secretion after glucose stimulation, compared to mice engrafted with wild type ESC and iPSC controls (Figure 3D). Importantly, mice with PTV1C and PTV2C gene-corrected transplants showed physiological decreases of circulating human C-peptide during fasting and increased C-peptide in response to glucose, while mice with uncorrected mutant cells did not (Figure 3E, F). However, the absolute serum concentration of human C-peptide in mice with gene-corrected cells did not reach those of MEL-1 cells, and were not sufficient to fully substitute for the endogenous mouse beta cells (Figure S5A). We attribute this partial substitution to the variability in iPSC quality [64]. Importantly, we did not ablate mouse beta cells in any of these studies. Streptozotocin can be dosed to preferentially kill endogenous mouse beta cells, but not transplanted human cells [19,69] Here, we were concerned that the proposed increased ER stress-susceptibility of the mutant cells would render them more sensitive to the STZ, confounding subsequent inferences regarding effects of the mutations on cell-autonomous *in vivo* functions of these cells.

We also measured serum glucose concentrations during intraperitoneal GSIS. Mice transplanted with PTV cells had higher serum glucose concentrations at 30 min post injection than mice with either MEL-1 grafts or with control iPS grafts (Figure S5B). Random glucose concentrations were lower in mice engrafted with control grafts derived from Mel1-WT/WT-iPSC compared to those bearing PTV grafts (Figure S5C). The disparity in glucose concentration thresholds for insulin secretion between human and mouse islets could underly this observation. Notably, human islets have a glucose—dependency curve shifted to lower concentrations, with a threshold of $\sim$54—72 mg/dL compared to $\sim$90 mg/dL for mouse islets [2,54]. This moves mouse blood glucose levels lower than usually observed in mice, which others also have documented [36].

We also transplanted NSG mice with Mel1 hESCs carrying the PTV1 mutation; controls were grafted with Mel1-WT cells (Figure 2C). As noted, Mel1 cells have only one functional *INS* allele as the other allele is null by virtue of insertion of GFP. Hence the Mel1 cells are all hemizygous for *INS*. No circulating human C-peptide was detected in mice engrafted with Mel1-PTV1 cells (Figure 3G), and no human insulin was detected during an GSIS during which wild type grafts produced concentrations of insulin (Figure 3H). These data indicate that the PTV1 allele does not produce secretable insulin (Figure 3C).

2.6. Loss of *INS* mutant beta-like cells after transplantation is associated with ER stress

We assessed the impact of nominal ER stress on survival of PTV1 and PTV2 beta cells after grafting. We compared grafted PTV1 and PTV2 beta cells with their corresponding corrected and wild-type control beta cells at 7 months post transplantation. We observed a severe

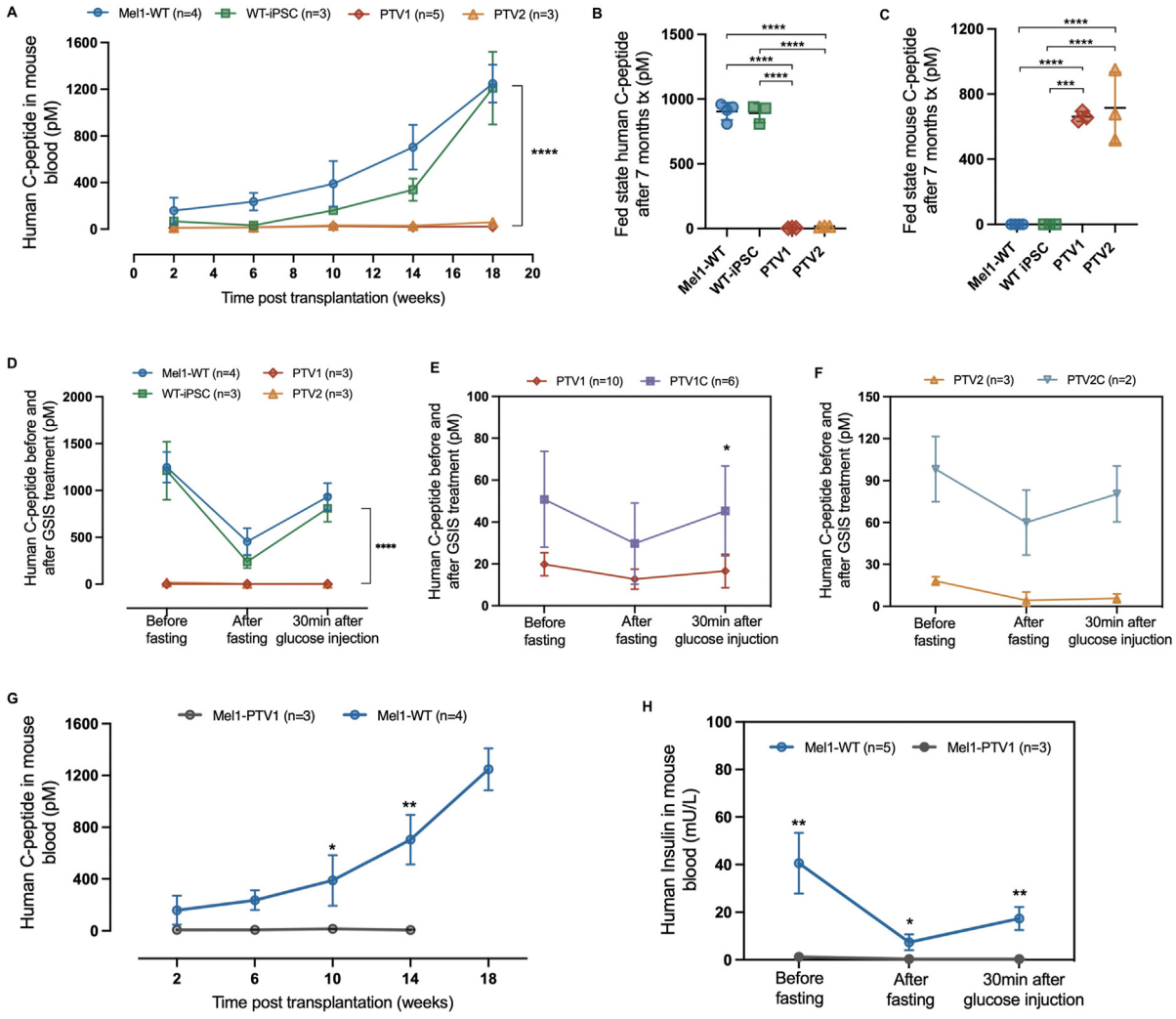

Figure 3: PTV SC-islets fail to secrete insulin and are unable to respond to glucose challenge in mice. (A) Human specific C-peptide levels(pM) in WT-iPSC (INSwt/wt), Mel1-WT (INSgfp/wt), PTV1 (INSptv1/wt) and PTV2 (INSptv2/wt) in plasma of mice engrafted with SC-islets. Human **(B)** and Mouse **(C)** fed state C-peptide levels(pM) after 7 months of transplantation. (Tx: Transplantation). Individual data points presented. One-way ANOVA and Tukey's multiple comparisons test. **(D–F)** Human C-peptide (pM) measured during glucose-stimulated insulin secretion (GSIS) at 7 months post-transplantation. Mice were injected IP with 2 g of glucose/kg body mass after overnight fasting (16 h). **(G)** Measurements of human specific C-peptide levels(pM) in Mel1-WT ($INS^{+/GFP}$) and Mel1-PTV1 ($INS^{PTV1/GFP}$) SC-islets engrafted mice blood after transplantation. **(H)** Human Insulin (mU/L) measured during glucose-stimulated insulin secretion (GSIS) at 7 months post-transplantation. Mice were injected IP with 2 g of glucose/kg body mass after overnight fasting (16 h). Data plots are presented as mean ± SEM. Two-way ANOVA test with *P < 0.05, **P < 0.01, ***P < 0.001, ****P < 0.0001.

reduction in the percentage of C-peptide-expressing cells or Insulin producing cells in the mutants (Figures 4A, B and S6A and B). However, at the time of initial transplantation, these alterations had not yet occurred, as the differentiation efficiency remained equivalent between mutant subjects and control groups (Figure 1E, F). Interestingly, most of the limited number of C-peptide-expressing cells in PTV1 and PTV2 grafts were immunopositive for the ER stress marker BIP, in contrast to much lower frequency in gene-corrected beta cells or uncorrected control cells (Figures 4A, C and S6A and C). Specifically, 64% and 67%, respectively of PTV1 and PTV2 C-peptide positive cells co-expressed BIP. Such double-positive cells were much rarer in control (3.50%) and corrected isogenic PTV1C (8.28%) and PTV2C (0.36%) cells (Figure 4C).

Introduction of the PTV1 mutation in Mel1 cells also reduced the number of C-peptide positive cells in grafts, and increased the BIP+C-peptide+ population from zero to 80% (Figure S6A and C). These results (Figure 4B) indicate significant beta cell loss resulting from the presence of the mutant *INS* alleles.

We evaluated the possibility that apoptosis may contribute to beta cell loss in mutant beta cells, we observed TUNEL-positive, C-peptide-producing cells in PTV cells after 27 days of *in vitro* differentiation (Figure S6D and E). However, gene-corrected isogenic control cells, did not significantly reduce apoptosis, suggesting that apoptosis observed may also be due to other causes, including spontaneous cell death (Figure S6D and E). Apoptosis was nearly undetectable in transplanted beta cells at seven months after *in vivo* engraftment (Figure S6F). Our findings are thus consistent with prior observations, that the loss of beta cells through apoptosis is not the primary mechanism in PNDM. This raises the question of whether other mechanisms might contribute to beta cell loss.

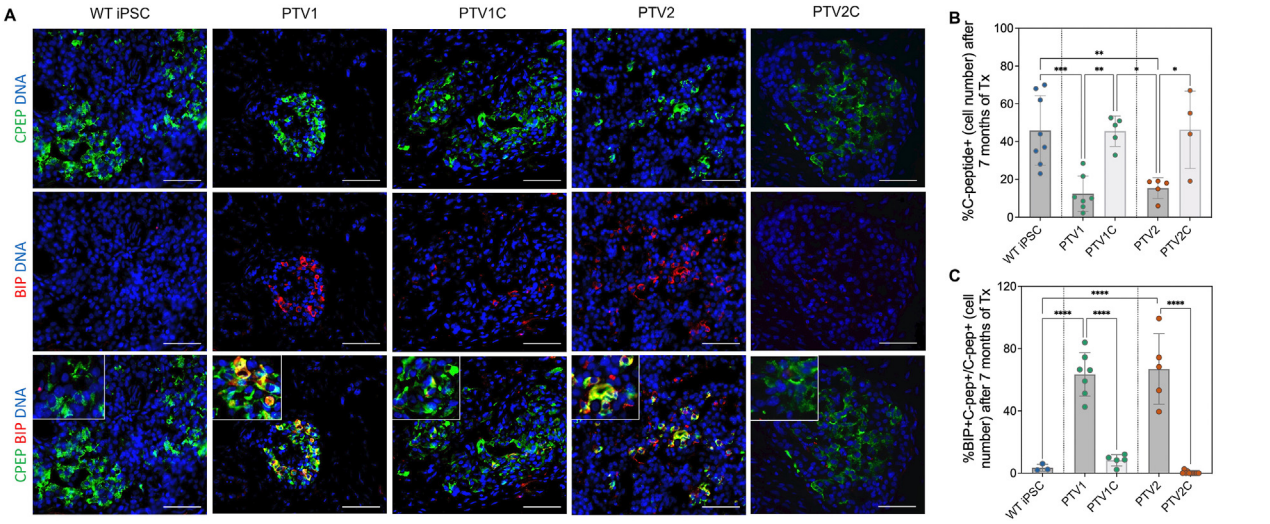

Figure 4: Increased expression of ER-stress markers grafts with PTV mutations. (A) Immunohistochemistry showing expression of ER stress marker-BIP in WT iPSC, PTV1, PTV1C, PTV2, and PTV2C SC-islets excised at 7 months post-transplantation. Scale bar: 50 μm. **(B)** Quantification of percentage of C-peptide+ cells of total graft cells quantified by Hoechst staining. The C-peptide antibody used detects both C-peptide and aa 33–63 of proinsulin. n = 3–4 independent transplanted mice per cellular genotype. 1-2 sections per mouse were analyzed, and the data points represent the percentage of C-peptide producing cells calculated from each section. **(C)** Quantification of colocalization of C-peptide+ and BIP+.The C-peptide antibody used detects both C-peptide and aa 33–63 of proinsulin. n = 3–4 independent transplanted mice per cellular genotype. Data were quantified by cell numbers and presented as mean ± SEM. One-way ANOVA test with *P < 0.05, **P < 0.01, ***P < 0.001, ****P < 0.0001.

2.7. Beta cells with INS mutation lose their identity after transplantation as a consequence of dedifferentiation

We immunostained stem cell-derived beta cell clusters for the presence of the alpha cell marker, glucagon, and assessed the ratio of C-peptide+ cells to Glucagon+ cells before and after 7 months of transplantation. Both controls (WT-iPSC) and corrected isogenic controls had similar percentage of C-peptide positive cells as a fraction of total cells prior to transplantation (Figure 5A, C). There was a ∼70% reduction of c-peptide positive beta-like cells in PTV1 and PTV2 mutant grafts at 7 months post-transplantation (Figure 5B, C). The ratio of proinsulin or C-peptide-positive cells/Glucagon-positive cells was approximately 1.6 in isogenic corrected and WT groups both before and after transplantation. In contrast, PTV1 and PTV2 grafts exhibited a decline in this ratio: decreasing from 1.7 (PTV1) and 1.5 (PTV2) before transplantation, to 0.5 (PTV1, P = 0.002) and 0.4 (PTV2, P = 0.012) at 7 months post-transplantation (Figure 5A, B and D). We observed the most significant reduction in this ratio in Mel1-PTV1 grafts, decreasing from 1.7 to 0.1 after 7 months of transplantation (P < 0.0001) (Figure S7A and B).

Specific factors can trigger loss (dedifferentiation) of mature beta cell identity. These include: oxidative stress [35,68], ER stress [11], inflammation [46] and hypoxia [49]. We performed immunoreactivity assays for ALDH1A3 (Figures 6A and S8A), which is upregulated in diabetic beta cell failure [12,67]. The mean percentage of ALDH1A3-positive cells per block was elevated more than 3-fold in PTV grafts compared with controls (P = 0.0012 for Mel1-PTV1 vs Mel1-WT) and isogenic corrected controls (P < 0.001 for PTV1 vs PTV1C and P = 0.037 for PTV2 vs PTV2C) (Figures 6B and S8B). In PTV1 grafts, more than 30% of ALDH1A3+ cells expressed NKX6.1, a beta cell specification transcription factor; the percentage of ALDH1A3+NKX6.1+ cells in PTV1 grafts were about 17 times higher than in isogenic control grafts (P = 0.016) (Figure 6C). In PTV2 patient cells, total ALDH1A3+ cells and ALDH1A3+ cells co-expressing NKX6.1 were also reduced after gene correction, although the difference was less significant (P = 0.036 in ALDH1A3+ cells and P = 0.038 in ALDH1A3+NKX6.1+ cells) (Figure 6C). To further examine whether insulin mutations are associated with molecular stigmata of de-differentiation, we examined iMel1-PTV1 grafts. Over 20% of ALDH1A3+ cells co-expressed NKX6.1, and the percentage of these double-positive cells were 4-fold higher than in Mel1-WT grafts (P < 0.0001) (Figure S8C). These findings are consistent with the inference that ALDH1A3 positive cells that are also positive for NKX6.1 are de-differentiated beta cells [12]. Of note is that the ALDH1A3+NKX6.1+ double-positive populations were no longer expressing insulin (Figures 6A and S8A).

ALDH1A3 is normally expressed in alpha cells, which are increased in T2D. Glucagon negative alpha cells are thought to be a consequence of beta cell de-differentiation [12]. The percentage of GCG-negative ALDHA3-expressing cells, representing a progenitor cell-like stage, was significantly increased in PTV grafts compared with their isogenic controls in both patient genotypes (P = 0.0013 for PTV1 vs PTV1C, P < 0.0001 for PTV2 vs PTV2C) (Figure 6D, E). A difference was also seen in Mel1-PTV1 grafts when compared with Mel1-Wt controls, though it did not reach statistical significance (Figure S8D and E).

Collectively, these results suggest that beta cells subjected to ER stress by misfolded insulin molecules exhibit heightened dedifferentiation, characterized by increased ALDH1A3 expression and loss of insulin expression.

3. DISCUSSION

We used patient-derived iPSCs as well as mutated human ESCs bearing two distinct clinically dominant *INS* mutations to identify genetically dominant derangements in proinsulin processing, proinsulin folding, ER trafficking and insulin production, associated with increased ER stress, beta cell dedifferentiation and death. These molecular-cellular phenotypes are consistent with the early onset insulin deficient phenotype of patients with these mutations.

Consistent with clinical data, stem cell-derived beta cell grafts harboring these specific mutations - in comparison to isogenic controls — produced less human insulin and showed reduced insulin-expressing

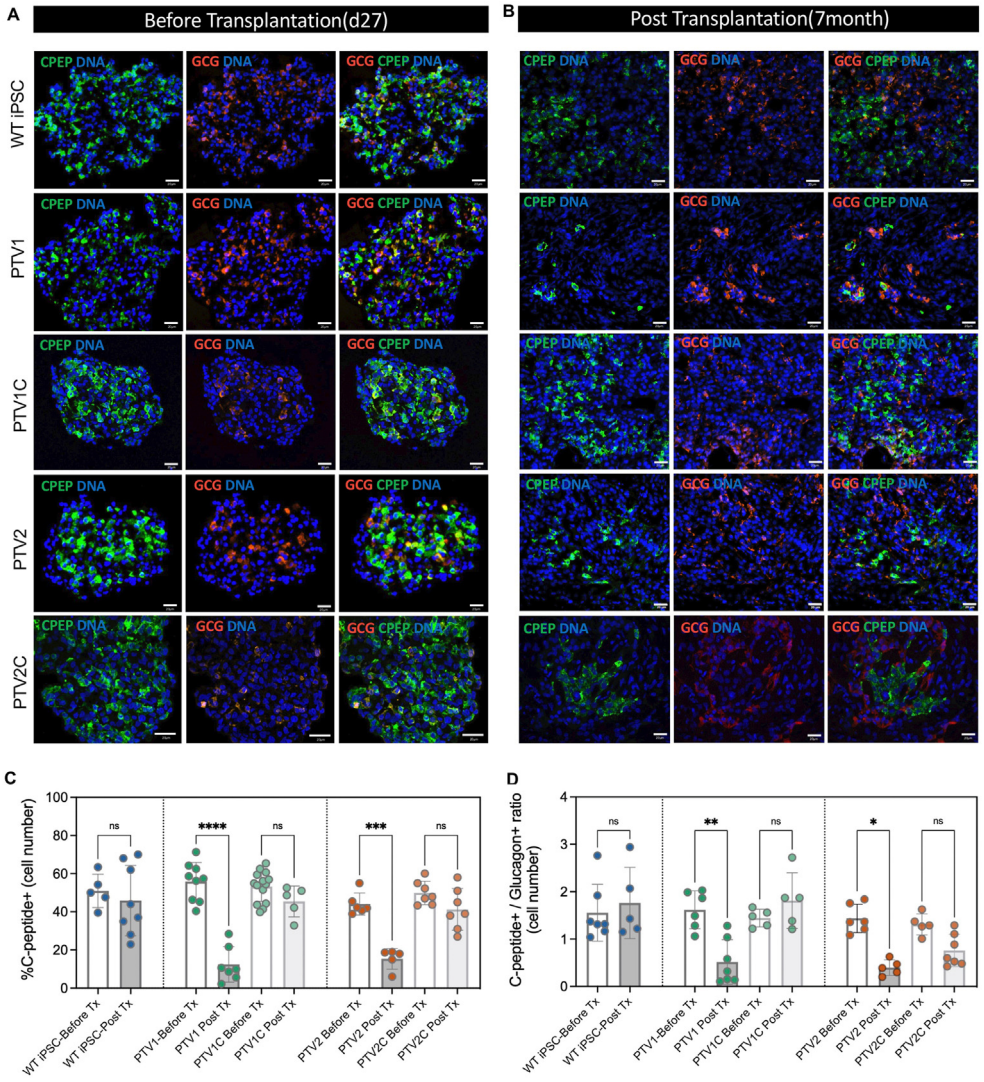

Figure 5: Loss of Insulin producing cells in PTV SC-islets engrafted to NSG mice. Immunohistochemistry for beta cell marker C-peptide and alpha cell marker Glucagon at d27 of *in vitro* differentiation. Scale bar: 20 μm. **(B)** Immunohistochemistry for beta cell marker C-peptide and alpha cell marker Glucagon at 7 months post transplantation. Scale bar: 20 μm. **(C)** Comparisons of percentage of C-peptide positive cells (%C-peptide+/Hoechest+) before(d27) and after transplantation (7months). **(D)** Ratio of insulin-producing cell number to Glucagon-producing cell number *in vitro* (27d) and *in vivo* (7months). The C-peptide antibody used detects both C-peptide and aa 33−63 of proinsulin. 3−4 transplanted mice were included, and cell numbers were counted from 1 to 3 sections obtained from each mouse. Each data point represented in the bar graph signifies the analysis conducted on a single section. Cell numbers are presented as mean ± SEM. Two-way ANOVA test with *P < 0.05, **P < 0.01, ***P < 0.001, ****P < 0.0001.

cell numbers after 7 months of transplantation. This decrease in the number of insulin-producing cells was due in part to cellular de-differentiation with loss of insulin protein production. From these findings, we infer that beta cells carrying the implicated neonatal diabetes *INS* mutations are subjected to proteotoxic misfolding of insulin precursors with attendant elevated ER stress and impaired insulin secretion. In addition, apoptosis, and beta cell de-differentiation reduce the number of insulin secreting cells. Thus, the clinical phenotype of severe insulin insufficiency results from convergent molecular and cellular events compromising the production of insulin.

Proinsulin misfolding has been proposed as a mechanism in PNDM [18,57]. These patients frequently segregate for heterozygous missense *INS* mutations leading to early onset (generally within the 1st 6 months of life) of permanent insulin deficiency [14,30]. Heterozygosity for null mutations of *INS* predisposes to diabetes, but of later onset and presumably in individuals with an enabling genetic background [10,51]. Thus, dominantly inherited *INS* mutations implicated in early onset insulin-dependent diabetes must have consequences for insulin processing and/or the viability of cells expressing the mutant peptide. This inference is supported by human clinical phenotypes as well as animal models including mouse and transgenic pigs [6,48,53]. In Akita mice expressing 3 copies of wild type *INS* (two *INS*1 and one *INS*2) and 1 copy of a misfolding *INS* mutation ($INS2^{+/C96Y}$), mutated proinsulin protein accounting for 36% of total translated proinsulin products was misfolded to higher-molecular-weight forms and that were associated with activation of the UPR [39]. We observed dimerized and trimerized proinsulin, as well as an elevated ratio of each higher-molecular-weight isoform to its monomer in cells expressing $L^{B15}Y^{B16}$delinsH (PTV1) or $Y^{B26}C$ (PTV2) heterozygous mutations. These mutations interfere with the cleavage and processing of proinsulin, and prohibit the formation of disulfide bonds in mature insulin [41,50]. A dominant-negative effect of the mutant insulin on

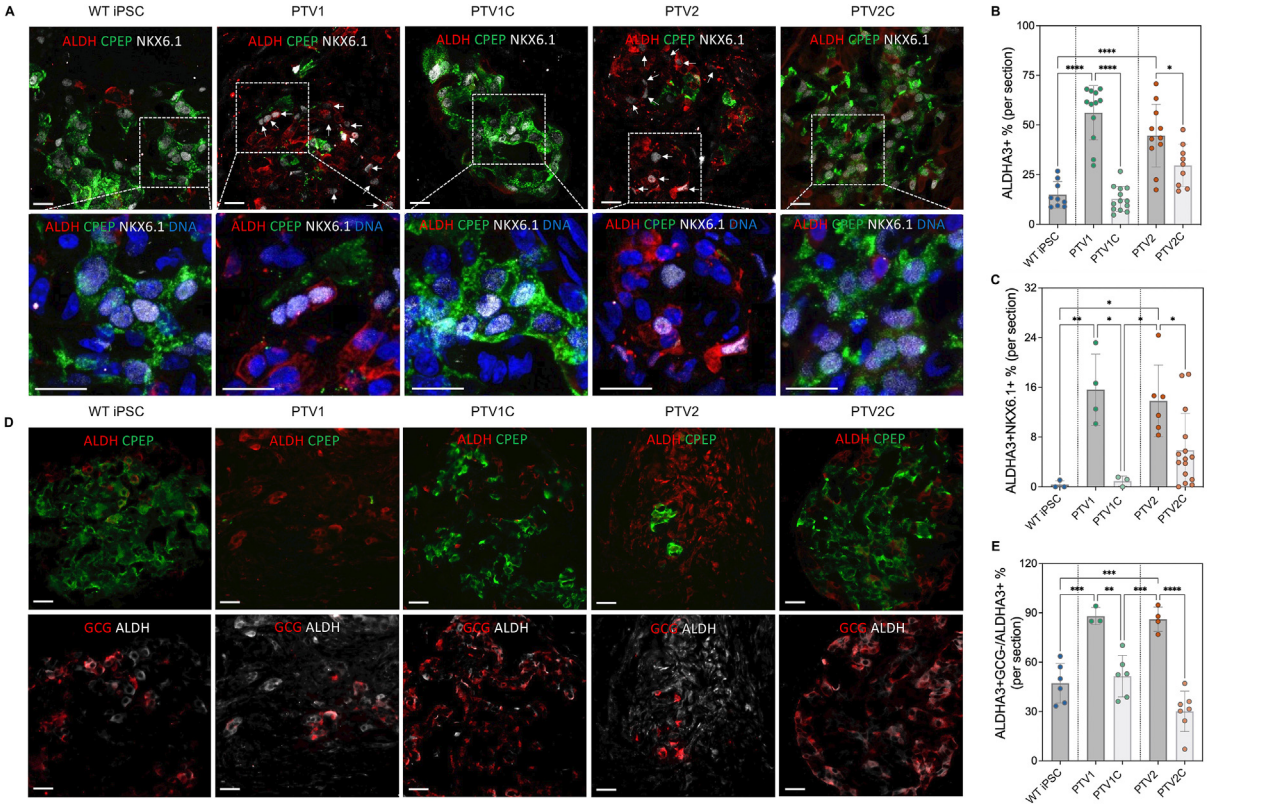

Figure 6: Increased beta cell dedifferentiation in stem cell-derived islet-like grafts carrying PTV mutations. (A) Immunohistochemistry for colocalization of dedifferentiation marker ALDH1A3 (ALDH) with beta cell marker C-peptide, NKX6.1 in 7-month-old grafts. Scale bar: 10 μm. **(B)** Percentage of ALDH1A3 positive cells. **(C)** Percentage of NKX6.1 positive cells co-expressing ALDH1A3, indicating dedifferentiated beta cells. **(D)** Immunohistochemistry for colocalization of dedifferentiation marker ALDH1A3 (ALDH) with C-peptide and alpha cell marker Glucagon in 7-month-old grafts. The C-peptide antibody used detects both C-peptide and aa 33—63 of proinsulin. Scale bar: 20 μm. **(E)** Quantitation of GCG-negative ALDH1A3 expressing cells. Each data point represents an independent frozen section randomly selected from 3 to 4 independent transplanted mice per cell genotype. Cell numbers are presented as mean ± SEM. One-way ANOVA test with *P $<$ 0.05, **P $<$ 0.01, ***P $<$ 0.001, ****P $<$ 0.0001.

processing of the wild type allele has been demonstrated [40]. This dominant effect *in vitro* in sc-beta cells, which resemble fetal-like beta cells [27]. This effect reduces, but does not eliminate all insulin secretion. Additional cellular consequences account for the long-term decline of insulin production after birth and diabetes. Heterozygous *INS* mutations may also cause diabetes with later onset in childhood, mimicking type 1 diabetes [7,77]. In these instances, C-peptide is usually detectable at the time of diagnosis and persists in gradual decline, suggesting that cell death and/or de-differentiation are contributing to the hypoinsulinemic phenotype. These long-term consequences are more accurately modeled by grafting of beta cells in mice (this study, and Ref. [21]).

We observed severe reductions of insulin-producing cells in both $L^{B15}Y^{B16}$delinsH and Y^{B26}C islet-like grafts at 7-months post transplantation. The majority of the surviving insulin-producing cells showed evidence of increased ER stress characterized by elevation of canonical molecular markers. However, given the impacts of $L^{B15}Y^{B16}$delinsH and Y^{B26}C mutations on *INS* folding we identified *ex vivo*, these findings are not surprising. Beta-cell apoptosis has been proposed as a main consequence of insulin misfolding and ER stress in many types of diabetes, including in T2D [37,48], MODY [70] and permanent neonatal diabetes (PND) [13,62]. The $L^{B15}Y^{B16}$delinsH mutation in patient PTV1 has been previously shown to cause apoptosis in cell-based assays [13]. Similarly, we detected increased apoptosis by TUNEL staining in stem cell derived beta cells *in vitro*. In contrast, we saw little apoptosis in transplanted beta-cells over a 7-month period. TUNEL may have missed a transient *in vitro* signal and *in vivo* adaptations may have mitigated longer term effects of the mutations. Compensatory reductions in (pro)insulin biosynthesis can reduce ER stress [55]. The Y^{B26}C mutation in PTV2 patients seems to have a greater effect on insulin synthesis and beta cell dedifferentiation than apoptosis. PNDM mutation *INS* C96R impacts a crucial cysteine residue responsible for the inter-chain disulfide bonds A7—B7; higher levels of ER stress were observed both *in vitro* and *in vivo* models of this mutation [5]. These findings are consistent with a modest activation of the unfolded protein response (UPR) noted in our study. But no increase in apoptosis was noted at any stage of differentiation in *INS* C96R cells [5]. Apoptosis may not be the primary cause of loss of beta cell function in PNDM caused by insulin mutations.

Here we have identified beta cell dedifferentiation as an important possible mechanism for loss of beta cell function in PNDM due to dominant/negative *INS* mutations as reflected in the presence of indicative molecular signatures: ALDH1A3+NKX6.1+ and ALDH1A3+ GCG-cells in SC-islet-like grafts after long term *in vivo* maturation. In agreement with a recent study showing a significant increase of Aldh1a3+ cells in islets of Akita mice at 5 months after birth, we found a distinct increase of Aldh1a3 expression in mutant transplants after months of *in vivo* maturation [34]. Upregulation of ALDH1A3 has been confirmed as a signature of dedifferentiation in human T2D diabetes islets, but has not been previously shown to occur in *INS* mutated human islets, or associated with ER stress caused by protein misfolding. Stem cell models of beta cell dysfunction involving ER stress

have been previously reported [5,56], but were not examined for evidence of de-differentiation. Though our stem cell model uses cells that are not fully mature at the time of transplantation, and thus may be less stable in their identity, this model system is still likely relevant to the disease in patients. During normal development, cells progress from immature to mature and de-differentiation triggered by mutant insulin may contribute to lower beta cell mass in neonatal diabetes patients. Our data implicate beta cell de-differentiation as a proximate mechanism for the beta cell failure characteristic of PNDM resulting from dominant-negative *INS* mutations. Hyperglycemia-induced ER stress is characteristic of T2D [37], and likely contributes to beta cell de-differentiation. Other genetic forms of neonatal diabetes due to explicit ER stress, including Wolfram and Wolcott—Rallison syndromes [61] may also be associated with beta cell de-differentiation. ER stress — perhaps depending on intensity and duration — can have various outcomes, including beneficial ones, such as cell proliferation [58,59]. In the case of insulin folding mutation, which appear to cause relatively modest ER stress levels, but over long-time frames, a prevalent consequence is de-differentiation.

Our results have implications regarding the biology of diabetes at several levels. They are consistent with recent suggestions that therapeutic Inhibition of ALDH1A3 might be useful to mitigate loss of functional beta cells in diabetes [60]. They also point to the likely clinical utility of isogenic stem cell lines in the creation of genetically "corrected" beta cells for transplantation in patients with monogenic etiologies of diabetes. However, such therapeutic advances will also require parallel improvements in iPSC reprogramming and quality control, as the differentiation potential of iPSCs to insulin producing cells often remains very variable (this study & Ref. [63]). And they again emphasize the utility of human stem cell-derived beta cells - and their *in vitro* and *in vivo* analyses — in understanding the molecular physiology of specific genetic derangements leading to clinical diabetes [21,56].

4. MATERIALS AND METHODS

4.1. Patients and cell lines

This study includes 10 human cell lines: a. 4 human embryonic stem cell lines (Mel1-WT: $INS^{+/GFP}$, Mel1-PTV1: $INS^{PTV1/GFP}$, Mel1-PTV2: $INS^{PTV1/GFP}$, Mel1-INS KO: $INS^{-/GFP}$). Mel1-WT was generated previously [45]; the other three were gene-edited using CRISPR/Cas9. b. 6 human pluripotent stem cell lines: (WT-iPSC: $INS^{+/+}$, PTV1: $INS^{PTV1/+}$, PTV2: $INS^{PTV2/+}$, PTV1C1: $INS^{+/+}$, PTV1C2: $INS^{+/+}$, PTV2C: $INS^{+/+}$). WT-iPSC was derived from a healthy donor (cell line 1159) [73]; PTV1 and PTV2 were reprogrammed from 2 PNDM patients as described in Results. 2 isogenic controls denominated PTV1C1 and PTV1C2 were corrected from PTV1 and another isogenic control PTV2C was corrected from PTV2. iPSCs derived from healthy or diabetic donors were reprogrammed from fibroblasts using mRNA reprogramming kit [43]. Additional details including cell lines, gRNAs, ssDNA templates and PCR primers are provided in Tables S3 and S4.

Cell lines were karyotyped by G band karyotyping by Cell Line Genetics. Karyotyping was also performed using low pass whole genome sequencing. Libraries were prepared using the Illumina DNA prep kit (catalog 20060059). Sequencing was performed using Illumina HiSeq 2500 with 2 × 150 bp configuration. Sequenced samples were analyzed using bwa aligner (v.0.7.17), samtools (v.1.11), and R package QDNAseq (v1.26.0.) Karyotypes were inspected using quantification of read numbers with a bin size of 500 kb.

Human fibroblasts were obtained after informed consent of the legal guardians of the patient at Salesi Hospital. Samples were de-identified and numbered PTV1, PTV2. Genetic analysis and use of patient samples in research was done with IRB approval at the University of Rome Tor Vergata. Work with human pluripotent stem cell lines was reviewed and approved by the Columbia University Embryonic Stem Cell Committee.

4.2. INS variants correction by CRISPR/Cas9

CRISPR/Cas9 gene editing system was employed to correct 2 pathogenic variants of *INS* (PTV1: $L^{B15}Y^{B16}$delinsH, PTV2: $Y^{B26}C$) and to generate 3 corrected cell lines (PTV1C1, PTV1C2 and PTV2C). Guide RNAs against *INS* loci adjacent to the mutations were designed using the online tool (https://www.idtdna.com/pages/tools/alt-r-crispr-hdr-design-tool) and synthesized by IDT (Integrated DNA Technologies). gRNAs were then assembled in a backbone vector (gBlock) by PCR for further functional expression using the method of Gibson [20]. gBlocks, correction template composed of single strand DNA (IDT) and Cas9-GFP were then transfected into human iPSCs for *INS* mutation correction using embryonic stem cell Nucleofector Kit (VVPH-5012, Lonza). Transfected cells were cultivated in StemFlex medium (catalog #A3349401, Thermo Fisher Scientific) supplemented with 10 mmol/L ROCK inhibitor-Y26732 (catalog #S1049; Selleckchem). After 48 h of proliferation, GFP positive cells were sorted by flow cytometry facilities in Columbia stem cell core and seeded onto GelTrex (catalog A1413302, Thermo Fisher Scientific) coated plates. ROCK inhibitor was removed after 24 h and the medium was refreshed every other day until 2 weeks later. Each clone was picked up and analyzed by PCR and sanger sequencing to select corrected *INS* clones. Additional details including cell lines, gRNAs, ssDNA templates and PCR primers are provided in Tables S3 and S4.

4.3. Cell culture and SC-derived beta-cell differentiation

All iPSCs and ESCs employed in this paper were seeded on GelTrex-coated plates, cultured in StemFlex medium and passaged with TrypLE Express (catalog #12605036; Life Technologies) every 3—5 days. Undifferentiated cells were then cultivated following a step-wise differentiation protocol previously established by our lab [64]; graphics illustrating differentiation stages are provided in Figure S1A. Cells were aggregated into clusters at Pancreatic Progenitor stage and were collected for further analysis within pancreatic beta-cell stage on d27. Images showing GFP-positive insulin-expressing cells were captured by an OLYMPUS IX73 fluorescent microscope.

4.4. Flow cytometry analysis

The SC-derived islet-like clusters were dissociated into single cells on d27 of differentiation using TrypLE Express. Dispersed cells were suspended in 5% FBS-containing PBS buffer for further use. Cells were then fixed in 4% paraformaldehyde (PFA) for 10 min followed by permeabilization at 20 °C with cold methanol for 10 min. Primary antibodies were incubated with cells for 1 h at 4 °C with a dilution of 1:100 in 0.5%BSA. Secondary antibodies were incubated with cells at a dilution of 1:500 for 1 h at room temperature. Cells were washed twice between every step by 5% FBS-containing PBS buffer. Lastly, collected cells were filtered into a Falcon round-bottom 12 × 15 mm tube through the cell strainer cap (catalog #352235; Corning) and analyzed by flow cytometer in Columbia stem cell core. All staining was performed at 4 °C. Data analysis was performed on FlowJo Software. Refer to Table S5 for additional information of primary antibodies and Table S6 for secondary antibodies.

4.5. Immunohistochemistry

SC-derived islet-like clusters were collected at day 27 of culture and fixed with 4% PFA at room temperature for 10—20 min. Grafts were

retrieved from the NSG mice post 7 months of transplantation, fixed with 4% PFA at room temperature for 1 h. The next steps were performed according to our formerly published method [64]. Briefly, fixed clusters and grafts were washed twice by PBS and incubated with 30% sucrose overnight at 4 °C to dehydrate and precipitate clusters. Aggregated clusters were transferred into a cryomold and immersed with O.C.T. medium over dry ice for cryosection. The frozen blocks were cut into 5-μm sections sections for further immunostaining. Primary antibodies used with this assay are listed in Table S5, and secondary antibodies are listed in Table S6. Images were taken with an OLYMPUS IX73 fluorescent microscope or a ZEISS LSM 710 confocal microscope. Frozen sections stained with the same markers were performed simultaneously and imaged with same parameters settings to ensure reliable quantification and comparison. Imaging processing and later quantification were performed blind, without labels using Fiji Software. Cell numbers were counted manually to calculate the positive or negative cell populations in all immunostaining sections. Apoptosis analysis was carried out with TUNEL assay. Frozen sections were processed with TUNEL apoptosis detection kit-CF594 (catalog #30064, Biotium) following the manufacturer's instructions.

4.6. Western blotting

SC-derived islet-like clusters at d27 were collected into pre-chilled 1.5 ml tubes and lysed with RIPA at 4 °C for 30 min. Clusters were vortexed every 5 min to ensure sufficient lysis. Supernatants containing total protein were retrieved after centrifuge. Samples were resolved by SDS in 4–12% Bis–Tris NuPAGE gels under either non-reducing or reducing conditions and electrotransferred to nitrocellulose. Development of immunoblots used enhanced chemiluminescence, captured with a Fotodyne gel imager, quantified using Fiji software. Of note, anti-KDEL antibodies were used to detect both Grp94 and BIP. Moreover, the proinsulin antibody (DSHB, Cat# GS-9A8; RRID: AB_532383) is highly specific, binding solely to the B–C junction of human proinsulin, and it exhibits no cross-reactivity with insulin or C-peptide. Additional details including primary and secondary antibodies are provided in Tables S5 and S6.

4.7. Metabolic labeling and immunoprecipitation

The pulse-chase experiment was performed as described previously [24]. Briefly, SC-derived islet-like clusters at d27 were dissociated to ~2–4 million cells and then labeled with ^{35}S-Cys/Met by incubation with cysteine/methionine-absent media for 30 min and defined pulse chase times. Labeled cells were washed with PBS containing 20 mmol/L N-ethyl maleimide (NEM) and then lysed in radioimmunoprecipitation assay buffer (25 mmol/L Tris, pH 7.5; 1% Triton X-100; 0.2% deoxycholic acid; 0.1% SDS; 10 mmol/L EDTA; and 100 mmol/L NaCl) with 2 mmol/L NEM and protease inhibitor. Centrifuged cell lysates, normalized to trichloroacetic acid precipitable counts and precleared with zysorbin, were immunoprecipitated and probed with anti-proinsulin and anti-insulin (B-chain) antibodies overnight at 4 °C. Immunoprecipitants were analyzed by nonreducing Tris–tricine–urea–SDS-PAGE, with phosphor imaging.

4.8. ELISA assays

Human proinsulin and insulin levels measured from cell content using human Proinsulin ELISA kit (Catalog #10-1118-01, Mercodia) and human Insulin ELISA kit (Catalog #10-1113-01, Mercodia). Human C-peptide level in mice serum sample were detected by Ultra-sensitive C-peptide ELISA kit (Catalog #10-1141-01, Mercodia). Mouse C-peptide levels were measured from plasma samples by using mouse C-peptide ELISA kit (Catalog #90050, Crystal Chem). All procedures were performed according to their manufacturing instructions.

4.9. Transplantation to NSG mice of SC-derived islet-like clusters and their *in vivo* assay

8-week-old male NOD-SCID-gamma (NSG) mice were purchased from Jackson Laboratories (catalog #005557) and housed at Columbia University Medical Center animal facility. Intra-leg quadriceps muscle transplantations were performed in 8 to10-week-old mice with approximately 2 million beta cells per mouse in accordance with published methods [21]. Briefly, SC-derived islet-like clusters were collected at d27 into a 1.5 ml pre-chilled tube with 50 μL Matrigel. Mice were anesthetized with isoflurane. Clusters mixed with gel were injected into the quadriceps using a 21-gauge needle. Fed state human C-peptide levels were detected and recorded (@ 4–5 pm) at 2 weeks post engraftment and every subsequent month. Glucose-stimulated insulin secretion was performed by fasting overnight (15–17 h) and 2 g/kg d-glucose intraperitoneal injection. Blood was collected from the tail vein into heparin-coated tubes at fed state, fasting state (0 min) and 30 min post injection (30 min). Whole blood glucose was also measured by glucometer at each time point. Supernatant plasma was separated through centrifugation at 2000 *g* for 15 min at 4 °C for human and mouse C-peptide measurement.

4.10. Statistical analysis

Statistical analysis was performed with Prism software (GraphPad Prism 9, GraphPad Software, Inc.). Differences between experimental groups were tested by 2-tailed unpaired or paired t test and by one-way or two-way ANOVA followed by Tukey's multiple-comparison test and presented as mean ± standard error of mean (SEM). The differences observed were considered statistically significant at the 5% level and annotated: *$P < 0.05$, **$P < 0.01$, ***$P < 0.001$, ****$P < 0.0001$.

MANUSCRIPT PREPARATION

This manuscript was prepared in part using solar electricity collected with a V250 Voltaic Systems solar panel and external laptop battery for a MacBook Pro between sea level in NYC and 17,200 feet (High Camp) in Denali National Park in the United States. Figure schematics were prepared using Biorender. ChatGPT was used to consider alternate synonymous wording of text.

AUTHOR CONTRIBUTIONS

LS, YZ, CUN, FB, PA and DE conceived, discussed and designed the study. LS and YZ carried out PTV1 patient-derived iPSCs relative experiments, YZ performed most PTV2 patient-derived iPSCs and Mel1-ESCs relative experiments, combined and analyzed all data, and wrote the manuscript with contributions from LS and DE, as well as from LH, PA and FB. LH and PA performed Western Blot experiments, design and interpretation. QD performed mice transplantation experiments, *in vivo* measurement and immunostaining for PTV2C grafts and Mel1-PTV1 grafts. YY assisted with generating mutated Mel1 cell lines, performed relative differentiation experiments and corresponding immunohistochemistry experiments. SX performed library preparation and karyotype analysis using sequencing read quantification. RV performed iPS reprogramming. RL contributed supervision. CUN conducted initial studies on iPS derivation, correction and differentiation. FB coordinated human subject research. DE provided support, and supervision throughout the study.

ACKNOWLEDGMENTS

This research was supported by the American Diabetes Association (grant #1-16-ICTS-029) and the NYSTEM IDEA award # C029552, Leona and Harry Helmsley Charitable Trust, Helmsley Trust Diabetes Cell Repository, the Juvenile Diabetes Research Foundation (JDRF), the Naomi Berrie Foundation program for Cellular Therapies of Diabetes, F.B. was supported by and the Italian Ministry of Health (project PE-2011-02350284). The contributions of P.A. and L.H. were supported by NIH R01 DK48280. These studies used the resources of the Herbert Irving Comprehensive Cancer Center Flow Cytometry Shared Resources funded in part through Center Grant P30CA013696, and the Diabetes Research Center Flow Core Facility funded in part through DRC Center Grant (5P30DK063608) and the MBMG Core in the New York Nutrition and Obesity Research Center (5P30DK026687). YZ was supported by a China Scholarship Council PhD student fellowship. We thank Charles LeDuc for help with mouse studies, Rudolph Leibel for helpful input and critical reading of the manuscript, and Robin Goland for helpful discussions on beta cell replacement therapies. We appreciate Stefano Zucchini and Federica Ortolani for their clinical contributions to PTV1 and PTV2 patients.

DECLARATION OF COMPETING INTEREST

Authors declare no conflicts of interest.

DATA AVAILABILITY

No data was used for the research described in the article.

APPENDIX A. SUPPLEMENTARY DATA

Supplementary data to this article can be found online at https://doi.org/10.1016/j.molmet.2024.101879.

REFERENCES

[1] Abdelalim EM. Modeling different types of diabetes using human pluripotent stem cells. Cell Mol Life Sci 2020;786(78):2459—83. https://doi.org/10.1007/S00018-020-03710-9.

[2] Abdulreda MH, Rodriguez-Diaz R, Caicedo A, Berggren PO. Liraglutide compromises pancreatic β cell function in a humanized mouse model. Cell Metab 2016;23:541—6. https://doi.org/10.1016/J.CMET.2016.01.009.

[3] Alam M, Arunagiri A, Haataja L, Torres M, Larkin D, Kappler J, et al. Predisposition to proinsulin misfolding as a genetic risk to diet-induced diabetes. Diabetes 2021;70:2580—94. https://doi.org/10.2337/DB21-0422.

[4] Arunagiri A, Haataja L, Pottekat A, Pamenan F, Kim S, Zeltser LM, et al. Proinsulin misfolding is an early event in the progression to type 2 diabetes. eLife 2019;8. https://doi.org/10.7554/ELIFE.44532.

[5] Balboa D, Saarimäki-Vire J, Borshagovski D, Survila M, Lindholm P, Galli E, et al. Insulin mutations impair beta-cell development in a patient-derived iPSC model of neonatal diabetes. eLife 2018;7:1—35. https://doi.org/10.7554/eLife.38519.

[6] Blutke A, Renner S, Flenkenthaler F, Backman M, Haesner S, Kemter E, et al. The Munich MIDY Pig Biobank — a unique resource for studying organ crosstalk in diabetes. Mol Metab 2017;6:931—40. https://doi.org/10.1016/J.MOLMET.2017.06.004.

[7] Bonfanti R, Colombo C, Nocerino V, Massa O, Lampasona V, Iafusco D, et al. Insulin gene mutations as cause of diabetes in children negative for five type 1 diabetes autoantibodies. Diabetes Care 2009;32:123—5. https://doi.org/10.2337/DC08-0783.

[8] Brozzi F, Eizirik DL. ER stress and the decline and fall of pancreatic beta cells in type 1 diabetes. J Med Sci 2016;121:133—9. https://doi.org/10.3109/03009734.2015.1135217.

[9] Brusko TM, Russ HA, Stabler CL. Strategies for durable β cell replacement in type 1 diabetes. Science 2021;373:516—22. https://doi.org/10.1126/SCIENCE.ABH1657.

[10] Carmody D, Park SY, Ye H, Perrone ME, Alkorta-Aranburu G, Highland HM, et al. Continued lessons from the INS gene: an intronic mutation causing diabetes through a novel mechanism. J Med Genet 2015;52:612—6. https://doi.org/10.1136/JMEDGENET-2015-103220.

[11] Chen CW, Guan BJ, Alzahrani MR, Gao Z, Gao L, Bracey S, et al. Adaptation to chronic ER stress enforces pancreatic β-cell plasticity. Nat Commun 2022;131(13):1—18. https://doi.org/10.1038/s41467-022-32425-7.

[12] Cinti F, Bouchi R, Kim-Muller JY, Ohmura Y, Sandoval PR, Masini M, et al. Evidence of β-cell dedifferentiation in human type 2 diabetes. J Clin Endocrinol Metab 2016;101:1044—54. https://doi.org/10.1210/JC.2015-2860.

[13] Colombo C, Porzio O, Liu M, Massa O, Vasta M, Salardi S, et al. Seven mutations in the human insulin gene linked to permanent neonatal/infancy-onset diabetes mellitus. J Clin Investig 2008;118:2148. https://doi.org/10.1172/JCI33777.

[14] Dahl A, Kumar S. Recent advances in neonatal diabetes. Diabetes Metab Syndr Obes Targets Ther 2020;13:355. https://doi.org/10.2147/DMSO.S198932.

[15] De Franco E, Flanagan SE, Houghton JAL, Allen HL, MacKay DJG, Temple IK, et al. The effect of early, comprehensive genomic testing on clinical care in neonatal diabetes: an international cohort study. Lancet 2015;386:957—63. https://doi.org/10.1016/S0140-6736(15)60098-8.

[16] Edghill EL, Dix RJ, Flanagan SE, Bingley PJ, Hattersley AT, Ellard S, et al. HLA genotyping supports a nonautoimmune etiology in patients diagnosed with diabetes under the age of 6 months. Diabetes 2006;55:1895—8. https://doi.org/10.2337/db06-0094.

[17] Edghill EL, Flanagan SE, Patch AM, Boustred C, Parrish A, Shields B, et al. Insulin mutation screening in 1,044 patients with diabetes mutations in the INS gene are a common cause of neonatal diabetes but a rare cause of diabetes diagnosed in childhood or adulthood. Diabetes 2008;57:1034—42. https://doi.org/10.2337/db07-1405.

[18] Elizabeth Jane Besser R, Elizabeth Flanagan S, Gordon Mackay J, Karen Temple I, Shepherd Maggie H, Shields Beverley M, et al. Prematurity should not prevent genetic testing for neonatal diabetes. Pediatrics 2016;138. https://doi.org/10.1542/peds.2015-3926.

[19] Estilles E, Téllez N, Nacher M, Montanya E. A model for human islet transplantation to immunodeficient streptozotocin-induced diabetic mice. Cell Transplant 2018;27:1684—91. https://doi.org/10.1177/0963689718801006.

[20] Gibson DG, Young L, Chuang RY, Venter JC, Hutchison CA, Smith HO. Enzymatic assembly of DNA molecules up to several hundred kilobases. Nat Methods 2009;65(6):343—5. https://doi.org/10.1038/nmeth.1318.

[21] González BJ, Zhao H, Niu J, Williams DJ, Lee J, Goulbourne CN, et al. Reduced calcium levels and accumulation of abnormal insulin granules in stem cell models of HNF1A deficiency. Commun Biol 2022;5. https://doi.org/10.1038/S42003-022-03696-Z.

[22] Greeley SAW, Polak M, Njølstad PR, Barbetti F, Williams R, Castano L, et al. ISPAD Clinical Practice Consensus Guidelines 2022: the diagnosis and management of monogenic diabetes in children and adolescents. Pediatr Diabetes 2022;23:1188—211. https://doi.org/10.1111/PEDI.13426.

[23] Haataja L, Arunagiri A, Hassan A, Regan K, Tsai B, Dhayalan B, et al. Distinct states of proinsulin misfolding in MIDY. Cell Mol Life Sci 2021;78:6017—31. https://doi.org/10.1007/S00018-021-03871-1.

[24] Haataja L, Manickam N, Soliman A, Tsai B, Liu M, Arvan P. Disulfide mispairing during proinsulin folding in the endoplasmic reticulum. Diabetes 2016;65:1050—60. https://doi.org/10.2337/DB15-1345/-/DC1.

[25] Habeb AM, Al-Magamsi MSF, Eid IM, Ali MI, Hattersley AT, Hussain K, et al. Incidence, genetics, and clinical phenotype of permanent neonatal diabetes mellitus in northwest Saudi Arabia. Pediatr Diabetes 2012;13:499–505. https://doi.org/10.1111/J.1399-5448.2011.00828.X.

[26] Herbach N, Rathkolb B, Kemter E, Pichl L, Klaften M, Hrabé De Angelis M, et al. Dominant-negative effects of a novel mutated Ins2 allele causes early-onset diabetes and severe-cell loss in Munich Ins2 C95S mutant mice. Diabetes 2007;56:1268–76. https://doi.org/10.2337/db06-0658.

[27] Hrvatin S, O'Donnell CW, Deng F, Millman JR, Pagliuca FW, Dilorio P, et al. Differentiated human stem cells resemble fetal, not adult, β cells. Proc Natl Acad Sci U S A 2014;111:3038–43. https://doi.org/10.1073/PNAS.1400709111.

[28] Iafusco D, Massa O, Pasquino B, Colombo C, Iughetti L, Bizzarri C, et al. Minimal incidence of neonatal/infancy onset diabetes in Italy is 1:90,000 live births. Acta Diabetol 2012;49:405. https://doi.org/10.1007/S00592-011-0331-8.

[29] Iafusco D, Salardi S, Chiari G, Toni S, Rabbone I, Pesavento R, et al. No sign of proliferative retinopathy in 15 patients with permanent neonatal diabetes with a median diabetes duration of 24 years. Diabetes Care 2014;37:e181–2. https://doi.org/10.2337/DC14-0471.

[30] Iafusco D, Stazi MA, Cotichini R, Cotellessa M, Martinucci ME, Mazzella M, et al. Permanent diabetes mellitus in the first year of life, and the early onset diabetes study group of the Italian Society of Paediatric Endocrinology. Diabetologia 2002;45:798–804. https://doi.org/10.1007/s00125-002-0837-2.

[31] Ichi Nozaki J, Kubota H, Yoshida H, Naitoh M, Goji J, Yoshinaga T, et al. The endoplasmic reticulum stress response is stimulated through the continuous activation of transcription factors ATF6 and XBP1 in Ins2+/Akita pancreatic β cells. Genes Cells 2004;9:261–70. https://doi.org/10.1111/j.1356-9597.2004.00721.x.

[32] Izumi T, Yokota-Hashimoto H, Zhao S, Wang J, Halban PA, Takeuchi T. Dominant negative pathogenesis by mutant proinsulin in the Akita diabetic mouse. Diabetes 2003;52:409–16. https://doi.org/10.2337/DIABETES.52.2.409.

[33] Johannesson B, Sui L, Freytes DO, Creusot RJ, Egli D. Toward beta cell replacement for diabetes. EMBO J 2015;34:841–55. https://doi.org/10.15252/EMBJ.201490685.

[34] Kitakaze K, Oyadomari M, Zhang J, Hamada Y, Takenouchi Y, Tsuboi K, et al. ATF4-mediated transcriptional regulation protects against β-cell loss during endoplasmic reticulum stress in a mouse model. Mol Metab 2021;54. https://doi.org/10.1016/J.MOLMET.2021.101338.

[35] Kitamura YI, Kitamura T, Kruse JP, Raum JC, Stein R, Gu W, et al. FoxO1 protects against pancreatic beta cell failure through NeuroD and MafA induction. Cell Metab 2005;2:153–63. https://doi.org/10.1016/J.CMET.2005.08.004.

[36] Kroon E, Martinson LA, Kadoya K, Bang AG, Kelly OG, Eliazer S, et al. Pancreatic endoderm derived from human embryonic stem cells generates glucose-responsive insulin-secreting cells in vivo. Nat Biotechnol 2008;264(26):443–52. https://doi.org/10.1038/nbt1393.

[37] Laybutt DR, Preston AM, Åkerfeldt MC, Kench JG, Busch AK, Biankin AV, et al. Endoplasmic reticulum stress contributes to beta cell apoptosis in type 2 diabetes. Diabetologia 2007;50:752–63. https://doi.org/10.1007/S00125-006-0590-Z.

[38] Lipson KL, Fonseca SG, Ishigaki S, Nguyen LX, Foss E, Bortell R, et al. Regulation of insulin biosynthesis in pancreatic beta cells by an endoplasmic reticulum-resident protein kinase IRE1. Cell Metab 2006;4:245–54. https://doi.org/10.1016/J.CMET.2006.07.007.

[39] Liu M, Haataja L, Wright J, Wickramasinghe NP, Hua Q-X. Mutant INS-gene induced diabetes of youth: proinsulin cysteine residues impose dominant-negative inhibition on wild-type proinsulin transport. PLoS One 2010;5:13333. https://doi.org/10.1371/journal.pone.0013333.

[40] Liu M, Hodish I, Rhodes CJ, Arvan P. Proinsulin maturation, misfolding, and proteotoxicity. Proc Natl Acad Sci U S A 2007;104:15841. https://doi.org/10.1073/PNAS.0702697104.

[41] Liu M, Weiss MA, Arunagiri A, Yong J, Rege N, Sun J, et al. Biosynthesis, structure, and folding of the insulin precursor protein. Diabetes Obes Metab 2018;20:28. https://doi.org/10.1111/DOM.13378.

[42] Liu M, Wright J, Guo H, Xiong Y, Arvan P. Proinsulin entry and transit through the endoplasmic reticulum in pancreatic beta cells. Vitam Horm 2014;95:35–62. https://doi.org/10.1016/B978-0-12-800174-5.00002-8.

[43] Ma S, Viola R, Sui L, Cherubini V, Barbetti F, Egli D. β cell replacement after gene editing of a neonatal diabetes-causing mutation at the insulin locus. Stem Cell Rep 2018;11:1407–15. https://doi.org/10.1016/J.STEMCR.2018.11.006.

[44] Maxwell KG, Augsornworawat P, Velazco-Cruz L, Kim MH, Asada R, Hogrebe NJ, et al. Gene-edited human stem cell-derived β cells from a patient with monogenic diabetes reverse preexisting diabetes in mice. Sci Transl Med 2020;12. https://doi.org/10.1126/SCITRANSLMED.AAX9106.

[45] Micallef SJ, Li X, Schiesser JV, Hirst CE, Yu QC, Lim SM, et al. INSGFP/w human embryonic stem cells facilitate isolation of in vitro derived insulin-producing cells. Diabetologia 2012;55:694. https://doi.org/10.1007/S00125-011-2379-Y.

[46] Nordmann TM, Dror E, Schulze F, Traub S, Berishvili E, Barbieux C, et al. The role of inflammation in β-cell dedifferentiation. Sci. Rep 2017;71(7):1–10. https://doi.org/10.1038/s41598-017-06731-w.

[47] Ortolani F, Piccinno E, Grasso V, Papadia F, Panzeca R, Cortese C, et al. Diabetes associated with dominant insulin gene mutations: outcome of 24-month, sensor-augmented insulin pump treatment. Acta Diabetol 2016;53:499. https://doi.org/10.1007/S00592-015-0793-1.

[48] Oyadomari S, Koizumi A, Takeda K, Gotoh T, Akira S, Araki E, et al. Targeted disruption of the chop gene delays endoplasmic reticulum stress–mediated diabetes. J Clin Investig 2002;109:525. https://doi.org/10.1172/JCI14550.

[49] Puri S, Akiyama H, Hebrok M. VHL-mediated disruption of Sox9 activity compromises β-cell identity and results in diabetes mellitus. Genes Dev 2013;27:2563. https://doi.org/10.1101/GAD.227785.113.

[50] Qiao Z-S, Guo Z-Y, Feng Y-M. Putative disulfide-forming pathway of porcine insulin precursor during its refolding in vitro. https://doi.org/10.1021/bi001613r; 2001.

[51] Raile K, O'Connell M, Galler A, Werther G, Kühnen P, Krude H, et al. Diabetes caused by insulin gene (INS) deletion: clinical characteristics of homozygous and heterozygous individuals. Eur J Endocrinol 2011;165:255–60. https://doi.org/10.1530/EJE-11-0208.

[52] Redondo MJ, Hagopian WA, Oram R, Steck AK, Vehik K, Weedon M, et al. The clinical consequences of heterogeneity within and between different diabetes types. Diabetologia 2020;63:2040. https://doi.org/10.1007/S00125-020-05211-7.

[53] Renner S, Braun-Reichhart C, Blutke A, Herbach N, Emrich D, Streckel E, et al. Permanent neonatal diabetes in INS C94Y transgenic pigs. Disbetes 2013;62. https://doi.org/10.2337/db12-1065.

[54] Rodriguez-Diaz R, Molano RD, Weitz JR, Abdulreda MH, Berman DM, Leibiger B, et al. Paracrine interactions within the pancreatic islet determine the glycemic set point. Cell Metab 2018;27:549. https://doi.org/10.1016/J.CMET.2018.01.015.

[55] Ron D. Proteotoxicity in the endoplasmic reticulum: lessons from the Akita diabetic mouse. J Clin Investig 2002;109:443–5. https://doi.org/10.1172/JCI200215020.

[56] Shang L, Hua H, Foo K, Martinez H, Watanabe K, Zimmer M, et al. β-Cell dysfunction due to increased ER stress in a stem cell model of Wolfram syndrome. Diabetes 2014;63:923–33. https://doi.org/10.2337/DB13-0717.

[57] Shankar RK, Pihoker C, Dolan LM, Standiford D, Badaru A, Dabelea D, et al. Permanent neonatal diabetes mellitus: prevalence and genetic diagnosis in the SEARCH for diabetes in youth study. Pediatr Diabetes 2013;14:174–80. https://doi.org/10.1111/pedi.12003.

[58] Sharma RB, O'Donnell AC, Stamateris RE, Ha B, McCloskey KM, Reynolds PR, et al. Insulin demand regulates β cell number via the unfolded protein response. J Clin Investig 2015;125:3831–46. https://doi.org/10.1172/JCI79264.

[59] Snyder JT, Darko C, Sharma RB, Alonso LC. Endoplasmic reticulum stress induced proliferation remains intact in aging mouse β-cells. Front Endocrinol 2021;12. https://doi.org/10.3389/FENDO.2021.734079/FULL.

[60] Son J, Du W, Esposito M, Shariati K, Ding H, Kang Y, et al. Genetic and pharmacologic inhibition of ALDH1A3 as a treatment of β-cell failure. Nat Commun 2023;14. https://doi.org/10.1038/S41467-023-36315-4.

[61] Stone SI, Abreu D, McGill JB, Urano F. Monogenic and syndromic diabetes due to endoplasmic reticulum stress. J Diabetes Complicat 2021;35:107618. https://doi.org/10.1016/J.JDIACOMP.2020.107618.

[62] Støy J, Edghill EL, Flanagan SE, Ye H, Paz VP, Pluzhnikov A, et al. Insulin gene mutations as a cause of permanent neonatal diabetes. Proc Natl Acad Sci 2007;104:15040—4. https://doi.org/10.1073/pnas.0707291104.

[63] Sui L, Danzl N, Campbell SR, Viola R, Williams D, Xing Y, et al. β-Cell replacement in mice using human type 1 diabetes nuclear transfer embryonic stem cells. Diabetes 2018;67:26—35. https://doi.org/10.2337/DB17-0120.

[64] Sui L, Leibel RL, Egli D. Pancreatic beta cell differentiation from human pluripotent stem cells. Curr Protoc Hum Genet 2018;99. https://doi.org/10.1002/CPHG.68.

[65] Sui L, Xin Y, Du Q, Georgieva D, Diedenhofen G, Haataja L, et al. Reduced replication fork speed promotes pancreatic endocrine differentiation and controls graft size. JCI Insight 2021;6. https://doi.org/10.1172/jci.insight.141553.

[66] Sun J, Xiong Y, Li X, Haataja L, Chen W, Mir SA, et al. Role of proinsulin self-association in mutant INS gene—induced diabetes of youth. Diabetes 2020;69:954—64. https://doi.org/10.2337/DB19-1106/-/DC1.

[67] Talchai C, Xuan S, Lin HV, Sussel L, Accili D. Pancreatic β cell dedifferentiation as a mechanism of diabetic β cell failure. Cell 2012;150:1223—34. https://doi.org/10.1016/J.CELL.2012.07.029/ATTACHMENT/8E9EAEEC-C9A5-4769-834E-00CA39266D6B/MMC1.MP4.

[68] Tanaka Y, Gleason CE, Tran POT, Harmon JS, Robertson RP. Prevention of glucose toxicity in HIT-T15 cells and Zucker diabetic fatty rats by antioxidants. Proc Natl Acad Sci U S A 1999;96:10857—62. https://doi.org/10.1073/PNAS.96.19.10857.

[69] Tuch BE, Turtle JR, Simeonovic CJ. Streptozotocin is not toxic to the human fetal B cell. Diabetologia 1989;32:678—84. https://doi.org/10.1007/BF00274256.

[70] Wang J, Takeuchi T, Tanaka S, Kubo SK, Kayo T, Lu D, et al. A mutation in the insulin 2 gene induces diabetes with severe pancreatic β-cell dysfunction in the Mody mouse. J Clin Investig 1999;103:27. https://doi.org/10.1172/JCI4431.

[71] Weiss MA. Proinsulin and the genetics of diabetes mellitus. J Biol Chem 2009;284:19159. https://doi.org/10.1074/JBC.R109.009936.

[72] Wright J, Wang X, Haataja L, Kellogg AP, Lee J, Liu M, et al. Dominant protein interactions that influence the pathogenesis of conformational diseases. J Clin Investig 2013;123:3124—34. https://doi.org/10.1172/JCI67260.

[73] Yamada M, Johannesson B, Sagi I, Burnett LC, Kort DH, Prosser RW, et al. Human oocytes reprogram adult somatic nuclei of a type 1 diabetic to diploid pluripotent stem cells. Nature 2014;510:533—6. https://doi.org/10.1038/nature13287.

[74] Yong J, Johnson JD, Arvan P, Han J, Kaufman RJ. Therapeutic opportunities for pancreatic β-cell ER stress in diabetes mellitus. Nat Rev Endocrinol 2021;17:455. https://doi.org/10.1038/S41574-021-00510-4.

[75] Yoshinaga T, Nakatome K, Nozaki JI, Naitoh M, Hoseki J, Kubota H, et al. Proinsulin lacking the A7-B7 disulfide bond, Ins2Akita, tends to aggregate due to the exposed hydrophobic surface. Biol Chem 2005;386:1077—85. https://doi.org/10.1515/BC.2005.124/MACHINEREADABLECITATION/RIS.

[76] Yoshioka M, Kayo T, Ikeda T, Koizumi A. A novel Locus, Mody4, distal to D7Mit189 on chromosome 7 determines early-onset NIDDM in Nonobese C57BL/6 (Akita) mutant mice. Diabetes 1997;46:887—94. https://doi.org/10.2337/diab.46.5.887.

[77] Yu MG, Keenan HA, Shah HS, Frodsham SG, Pober D, He Z, et al. Residual β cell function and monogenic variants in long-duration type 1 diabetes patients. J Clin Investig 2019;129:3252—63. https://doi.org/10.1172/JCI127397.

